(one6G)

Taking communications
to the next level

Technical Report on the WG4 PoC:

ISAC-ENABLED DETECTION OF ANTENNA TILT FAILURES

TECHNICAL REPORT

November 2026

one6g.org

Executive Summary

This Technical Report presents the joint Proof of Concept (PoC) activity conducted by Turkcell 6GEN.LAB and Huawei Munich Research Centre (MRC) within the framework of one6G Working Group 4 (WI404). Moving beyond conventional outward-facing Integrated Sensing and Communication (ISAC) applications – such as environmental mapping and target tracking–this work introduces a novel inward-facing paradigm that utilizes ISAC as a sensor-free diagnostic tool for self-healing Radio Access Network (RAN) infrastructure. Specifically, the framework targets the autonomous detection and estimation of physical Antenna Tilt Failures (ATFs) caused by mechanical stress, windstorms, or long-term structural aging.

The PoC evaluation was executed in two distinct phases using Huawei MRC's monostatic cmWave ISAC testbed operating with a virtual MIMO architecture:

- Validation-Oriented Indoor Campaign: Conducted at a fixed 3-meter range with TV screen and desk table scatterers using different algorithms, this phase validated the point cloud data pipeline and confirmed that spatial point shifts projected onto 2D image frames map to physical tilt variations (yielding estimates such as -4.711°, -6.192° and -6.73° corresponding to real tilt value of -6.650°).
- Performance-Driven Outdoor Campaign: Conducted at an elevation of 15 meters across a near-field South Scene (19 m building facet) and an extended-range West Scene (30–146 m complex clutter), this phase benchmarked three 3D spatial point cloud algorithms (defined in the Annex). Among these, the 3D Correlation Search algorithm (with parabolic refinement) achieved considerable precision, recording a root mean square error of 0.358° in the South Scene and 0.456° in the West Scene.

Finally, this report outlines a Provisional Closed-Loop Automation Roadmap that connects algorithmic ATF estimation directly to internal Remote Electrical Tilt (RET) mechanisms. By converting fundamental 3D point cloud data into real-time misalignment telemetry, cellular operators can facilitate automated beam realignment. This approach eliminates the need for external IoT/gyroscope hardware CAPEX and reduces operational expenditure (OPEX) by minimizing manual site audits and drive-tests. The underlying 3D Point Cloud dataset has been published on the one6G repository under the ODC-By license to support standardized 6G research.

Table of contents

EXECUTIVE SUMMARY **2**

TABLE OF CONTENTS **3**

1. INTRODUCTION **4**

2. OVERVIEW OF THE POC STUDY AND THE EXPERIMENTAL SETUP **6**

2.1. Testbed Specifications 7

2.2. Dataset Generation and Storage 7

3. MEASUREMENT CAMPAIGNS, ALGORITHMIC FRAMEWORK AND RESULTS **9**

3.1. Validation-Oriented Indoor Test Campaign 9

3.2. Performance-Driven Outdoor Test Campaign 13

4. BUSINESS CASE: PROVISIONAL CLOSED-LOOP ROADMAP AND FINANCIAL IMPACT **17**

5. LIMITATIONS, OPEN CHALLENGES, AND PATH TO PRODUCTION READINESS **19**

6. CONCLUSIONS **20**

ACKNOWLEDGMENTS **21**

7. ANNEX: FLOWCHARTS AND DETAILED STEPS OF ATF ESTIMATION ALGORITHMS **22**

7.1. Annex-1: Algorithms Developed for Indoor Dataset 22

7.1.1. Algorithm-A: 2D Cross-Correlation-Based ATF Estimation *22*

7.1.2. Algorithm-B: Column-Wise Robust Median-Based ATF Estimation *23*

7.2. Annex-2: Algorithms Developed for Outdoor Dataset 24

7.2.1. Algorithm-C: Mean-Based ATF Estimation *24*

7.2.2. Algorithm-D: 3D Correlation Search *25*

7.2.3. Algorithm-E: Cluster Centroid Tracking and Matching *26*

ACRONYMS **28**

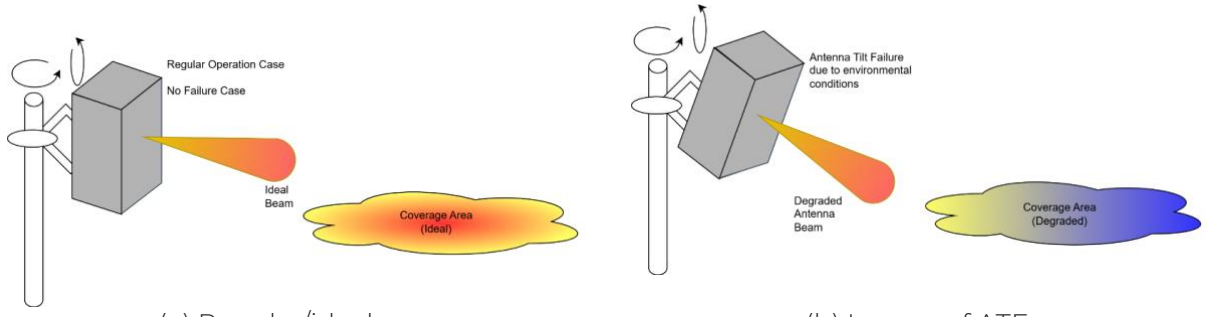
REFERENCES **29**

1. Introduction

This Technical Report of one6G Working Group 4 [1] summarizes the PoC implementation, experimental testbed setup, algorithmic framework, quantitative performance evaluation for ISAC-enabled physical antenna tilt failure (ATF) diagnosis, the provisional closed-loop automation roadmap with its financial impact, and the remaining challenges on the path to production readiness.

This section summarizes the technical core of the study: the experimental cmWave ISAC testbed, the algorithms proposed for antenna tilt failure (ATF) estimation, the outdoor validation results, the provisional closed-loop automation roadmap with its financial impact, and the remaining challenges on the path to production readiness.

Cellular network operators face a continuous operational challenge due to antenna misalignment caused by severe weather, mechanical stress, and physical degradation. Industry audits indicate that over 40% of active cellular antennas operate outside their designated mechanical tolerances, leading to severe coverage holes, throughput degradation, and inter-cell interference [2] , [3] . To illustrate the potential impact of mechanical degradations arising from various causes on the overall quality of service, the corresponding operational cases are depicted in Figure 1.



(a) Regular/ideal case (b) In case of ATFs

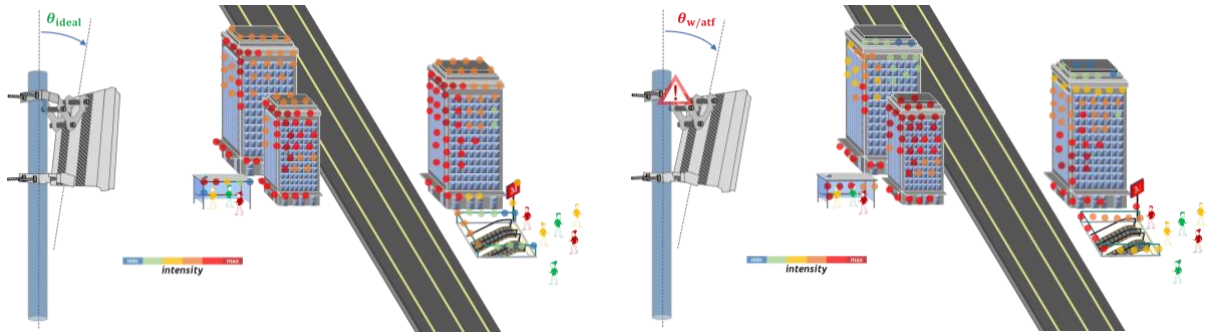
Figure 1 The degrading effects of unknown ATFs

In order to detect possible ATFs, traditional approaches rely on manual site visits, drive testing, or dedicated external physical sensors, incurring significant OPEX and management burden [4] . In addition to imposing significant operational overhead, such traditional approaches fail to mitigate user service disruptions encountered until ATFs are formally identified [5] The alternative of mounting dedicated hardware sensors, such as gyroscopes or IoT positioning modules, on every sector antenna is financially prohibitive and architecturally unscalable for ultra-dense 6G deployments (a “proactive scalability wall” driving CAPEX) [6] .

As a result of a core research question exploring whether ISAC's environmental sensing capabilities can detect variations caused by potential ATFs, this report highlights Integrated Sensing and Communication (ISAC) as a foundational enabler for autonomous self-healing networks [7] [8] . While current standardization efforts within 3GPP and ETSI predominantly focus on outward spatial sensing (e.g., target tracking, environmental mapping, vehicle localization), this PoC work aims to construct an ISAC-oriented inward sensing capability to detect and estimate the physical infrastructure integrity [9] [10]

By processing the monostatic 3D spatial returns generated by base stations (BSs), the proposed framework isolates fixed geometric anchors from dynamic transient noise, allowing for accurate physical ATF estimation without additional hardware cost. At this junction, assuming that uncontrolled antenna tilt variations resulting from physical impairments systematically alter environmental sensing data within ISAC-capable 6G networks, a reference baseline corresponding to the ideal state (e.g., average clutter heatmap, mean detection centroids) is established.

Subsequently, by analyzing the systematic variation in sensing signal intensity observed in periodic measurements of identical dimensionality relative to this reference, both the detection of ATFs and the estimation of the tilt shift value are projected to be feasible. Within this framework, the manifestation of post-ATF variations in periodic measurement data depends on the sensing methodology. For instance, if detection algorithms leveraging antenna tilt as prior knowledge are deployed, ATFs are prone to introducing coordinate shifts in the detected points, otherwise, ATFs will primarily alter the observed intensity at those detected locations.



(a) Regular/ideal case (b) In case of ATFs

Figure 2 The expected variation of detected points' scattering strengths

Figure 2-(a) illustrates the detection points and signal intensity values corresponding to stationary scatterers detected by an antenna operating at its nominal elevation tilt angle prior to an ATF. As observed in Figure 2-(b), an ATF induced by mechanical failure results in both spatial shifts in the detected coordinates and non-uniform variations in signal intensity values. Notably, while the signal intensity fluctuations - derived as long-term average representations to effectively mitigate transient spikes and short-term fading - demonstrate localized variations, their spatial distribution remains systematic rather than stochastic.

This report details the collaborative PoC execution, the dataset structure hosted under the ODC-By license on the one6G platform, the algorithmic diagnostic loop, and key experimental results.

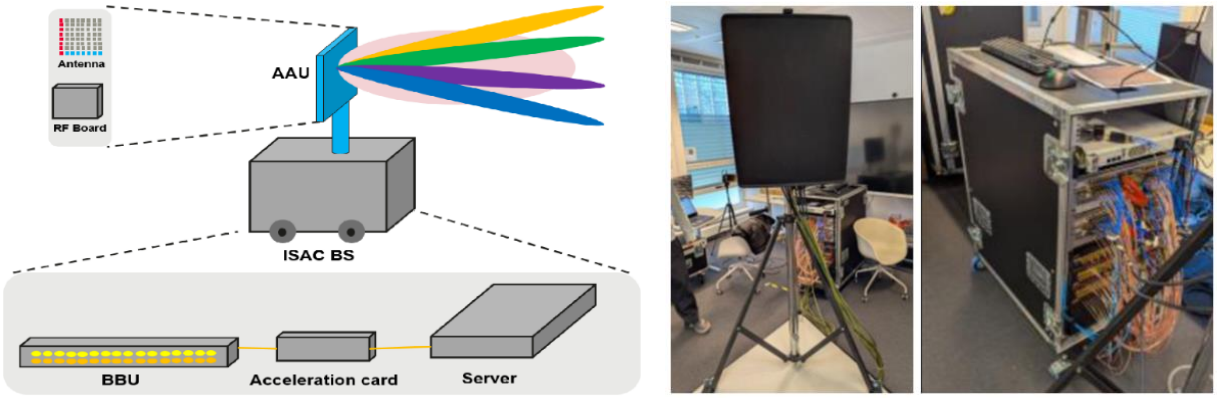
2. Overview of the PoC Study and the Experimental Setup

This section provides an overview of the PoC study, detailing the experimental architecture, RF transceiver specifications, and measurement campaign configurations utilized to validate inward-facing ISAC-based antenna tilt failure estimation. “Antenna Tilt Failure Estimation” is proposed as a new 6G ISAC use case by One6G member Turkcell, with the underlying motivation provided in the introduction. Following the interest of the one6G WG4 members a formal PoC has been started as Work Item 404. It was structured in two main scenarios:

- In scenario 1, several indoor measurements with different controlled antenna tilts and reference objects have been performed to study the general feasibility of the proposed idea. A test specification [11] composed jointly with all contributors of the PoC and aligned during the WG4 meetings, describes the motivation, the methodology and measurement setup in details. It can be accessed by all one6G members via the link: [https://shared.one6g.org/index.php/f/124200].
- In scenario 2, several outdoor measurements with more realistic scenarios have been considered. Mainly with higher antenna positions and more complex scenarios hosting multiple scatterers such as buildings, trees, cars and moving targets.

To validate the architectural concept on real-world hardware, a joint development was executed using the cutting-edge cmWave ISAC Testbed engineered by the Huawei Munich Research Centre (MRC) in collaboration with Turkcell 6GEN.LAB under one6G WG4 activities.

The experimental platform is a software defined monostatic cmWave ISAC testbed tailored for indoor and outdoor environmental reconstruction. It was already being used for the world's first large scale PoC sensing the inclination of the famous twin towers in Bologna / Italy during the one6G summit 2025 jointly performed by CNIT WiLAB and Huawei Advanced Wireless Lab of the Heisenberg Research Centre of Huawei located in Munich and presented in the one6G WG4 meetings as well as the one6G Open Lecture #12 [12]



(a) Architectural view of cmWave ISAC Testbed

(b) Antenna (left) and RF/BB Processing (right)

Figure 3 cmWave ISAC Testbed utilized for ATF estimation trials

The architectural diagram and the photographs corresponding to the antenna and the computation platform of the testbed are given in Figure 3-(a) and Figure 3-(b), respectively.

2.1. Testbed Specifications

The testbed is composed of an array-antenna platform used to illuminate the environment and to gather the echoing signals from the scatterers, and a rack cabinet housing the processing units dedicated to radio-frequency (RF), baseband (BB) and sensing operations. The active antenna unit (AAU) integrates an all-digital array operating in the cmWave band with an OFDM ISAC waveform, its elements arranged in a specialized L-shaped configuration of 32 transmitting and 32 receiving elements that balances high-resolution sensing with cost-effective design. Note that this design enables full aperture of the antenna for sensing while for full utilisation of MIMO for communication purposes an AAU with 32×32 TRX has to be considered [13] . With the assumption of an antenna spacing of half of the wavelength the angular resolutions of $1/16$ radians or 3.6 degree. The overall horizontal and vertical 3-dB beamwidth is equal to 100 degrees, and the equivalent isotropic radiated power is 12 dBm. A signal bandwidth (BW) of 400 MHz, the theoretical limits of the range resolutions where $dR{=}c/(2BW)$. With the given 400 MHz and the light speed c the minimum range resolution is 37.5 cm. 3GPP as main standardisation body for 6G has already decided to continue with OFDM for communication and sensing. Following that the cmWave prototype uses OFDM with a subcarrier spacing of 30 kHz.

Sensing data acquisition is governed by a pulsed-radar signaling scheme operating sequentially through alternating transmission (environmental illumination) and reception (echo listening) intervals. The duration dedicated to this combined illumination-listening cycle is reconfigurable within a window of 2 to 20 ms, providing operational flexibility to accommodate varying clutter densities and target range profiles.

In the experimental workflow, the overall sensing execution – encompassing transmission, echo capture, and subsequent baseband signal processing – is structured into discrete 3-second operational bursts. The testbed executes repetitive cycles where raw echo measurements are ingested, framed, and processed over each 3-second block, thereby establishing a consistent temporal baseline for spatial feature extraction while maintaining a controlled processing duty cycle. Further details regarding the testbed capabilities and the data processing and generation pipeline are documented in the presentation slides accessible on the one6G SharePoint portal: https://shared.one6g.org/index.php/f/128563.

2.2. Dataset Generation and Storage

Operating in a virtual MIMO configuration, each transmitting element sequentially radiates a burst of signals while all receiving elements simultaneously capture the spatial echoes. Through advanced post-processing of the received signals [14] Huawei's cmWave testbed prototype is capable of generating and storing a multi-faceted dataset consisting of:

- Raw Data: In-phase and Quadrature (I/Q) complex time-domain samples.
- Intermediate Representations: Channel State Information (CSI), Doppler spectrograms, and range-azimuth heatmaps.
- 3D Point Cloud Data: Reconstructed 3D spatial returns containing physical coordinate and intensity metrics.
- Ground Truth Metrics: Co-registered RGB camera images covering the antenna field of view (FoV) alongside physical tilt measurements. For this PoC study, rather than the raw I/Q signals, the derived 3D Point Cloud (PC) data (illustrated in Figure 4) is utilized as the primary diagnostic input.

From a structural perspective, the point cloud represents a finite set of discrete spatial returns, where each point p_k is defined by a multi-dimensional tuple: $p_k{=}[x_k, y_k, z_k, \rho_k]$. Here x_k, y_k and z_k

denote the 3D Cartesian spatial coordinates relative to the antenna phase center, while ρ_k represents the scattering intensity or reflectivity of the specific scatterer.

The temporal behavior of these scatterers defines their diagnostic reliability: static structures (e.g., building facets, rack cabinets) form geometric anchors whose apparent spatial displacement directly indicates physical tilt degradation, whereas dynamic targets (e.g., pedestrians, vehicles) create transient clutter. The utilization of this point cloud data varied across testing phases:

- Indoor Preliminary Validation Tests: Point cloud returns were projected onto 2D RGB camera frames to evaluate target mapping, verify spatial point cloud density, and enable online visual monitoring of spatial shifts under controlled tilt conditions. It should be noted that, the projected points/pixels do not contain the distinguishable scattering intensity information ρ_k.
- Outdoor Final Performance Evaluation: To evaluate real-world RAN self-diagnostic capabilities, the raw 3D point cloud matrices $N \times 4$ were directly ingested into post-processing diagnostic algorithms. Density-guided clustering (DBSCAN) was applied to isolate permanent structural anchors from transient dynamic clutter prior to tilt estimation.

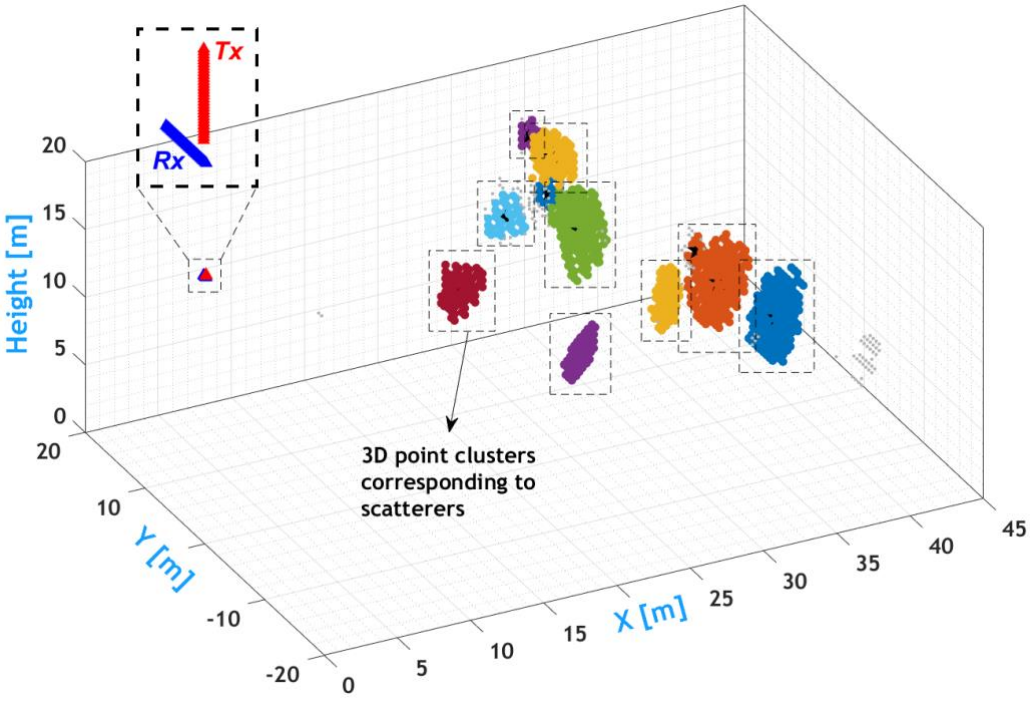


Figure 4 3D Point Cloud generated by cmWave ISAC Testbed

To support offline quality verification, research collaboration, and algorithm benchmarking, the high-quality datasets generated during these measurements have been uploaded to the one6G repository under the ODC-by license as part of TODSI. The dataset is accessible via the official one6G Sharepoint repository with the path working groups / WG4-Evaluation-Testbeds-Pilots / WG4-Workitems / WI404-PoC antenna tilt sensing with the URL https://shared.one6g.org/index.php/f/123404.

3. Measurement Campaigns, Algorithmic Framework and Results

This section presents the experimental measurement scenarios, data collection campaigns, developed diagnostic algorithms, and the resulting performance evaluations for ATF detection and estimation. To validate the proposed inward-facing ISAC framework, a two-phase campaign was executed, transitioning from controlled laboratory settings to real-world outdoor deployments:

1. Validation-Oriented Indoor Test Campaign: Focuses on verifying data pipeline integrity, confirming spatial point cloud resolution, and evaluating initial 2D cross-correlation (Algorithm-A) and median-based estimation (Algorithm-B) approaches under controlled indoor conditions.

2. Performance-Driven Outdoor Test Campaign: Evaluates real-world diagnostic capabilities by applying three algorithms – namely Mean-Based Estimation (Algorithm-C), 3D Correlation Search (Algorithm-D), and Cluster Centroid Tracking (Algorithm-E) – to benchmark estimation accuracy and Root Mean Square Error (RMSE) against structural clutter and extended target ranges.

3. Ground-Truth Benchmark Calibration: To establish physical ground-truth benchmarks across both campaigns, a commercial dual-axis digital inclinometer (Digi-Pas DWL-90Pro [15]) was mounted on the antenna bracket using its integrated magnetic base. The instrument provides an angular measurement resolution of $0.05°$ with a manufacturer-specified accuracy of $\pm 0.1°$ in the near-horizontal regime ($0° - 1°$) and $\pm 0.2°$ across the broader range ($1° - 89°$). Ground-truth tilt angles were logged wirelessly via a Bluetooth interface, eliminating physical contact during data acquisition and preventing inadvertent mechanical perturbations or structural vibrations on the antenna fixture.

3.1. Validation-Oriented Indoor Test Campaign

An initial laboratory test was conducted to verify the data structure and support the early development of post-processing solutions by the project partners. The test was intended to establish a baseline for the sensing data and provide an initial dataset for the development and validation of post-processing algorithms. For these preliminary validation tests, the antenna setup and scatterer positioning were arranged in accordance with the representative indoor layout depicted in Figure 5, where raw I/Q data and subsequent point cloud representations were sequentially generated via the cmWave testbed.

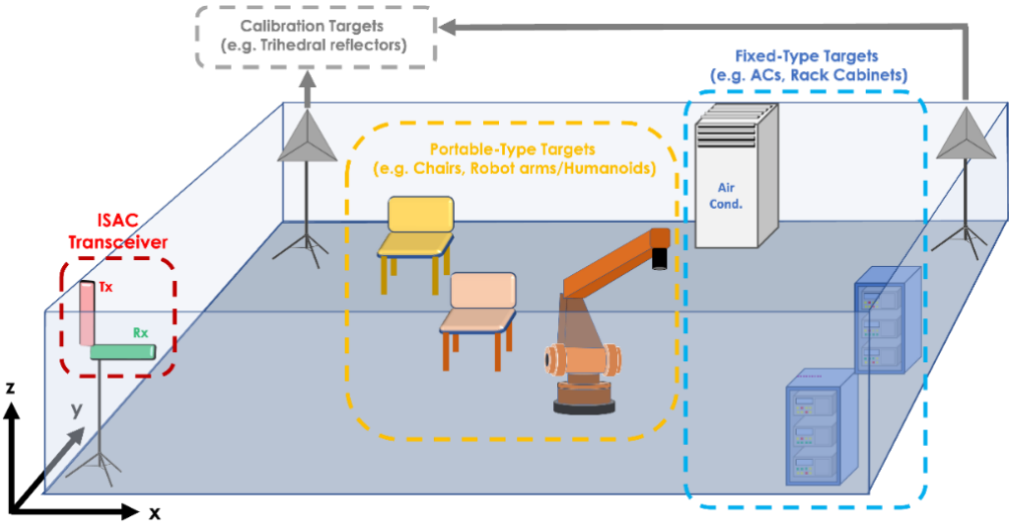


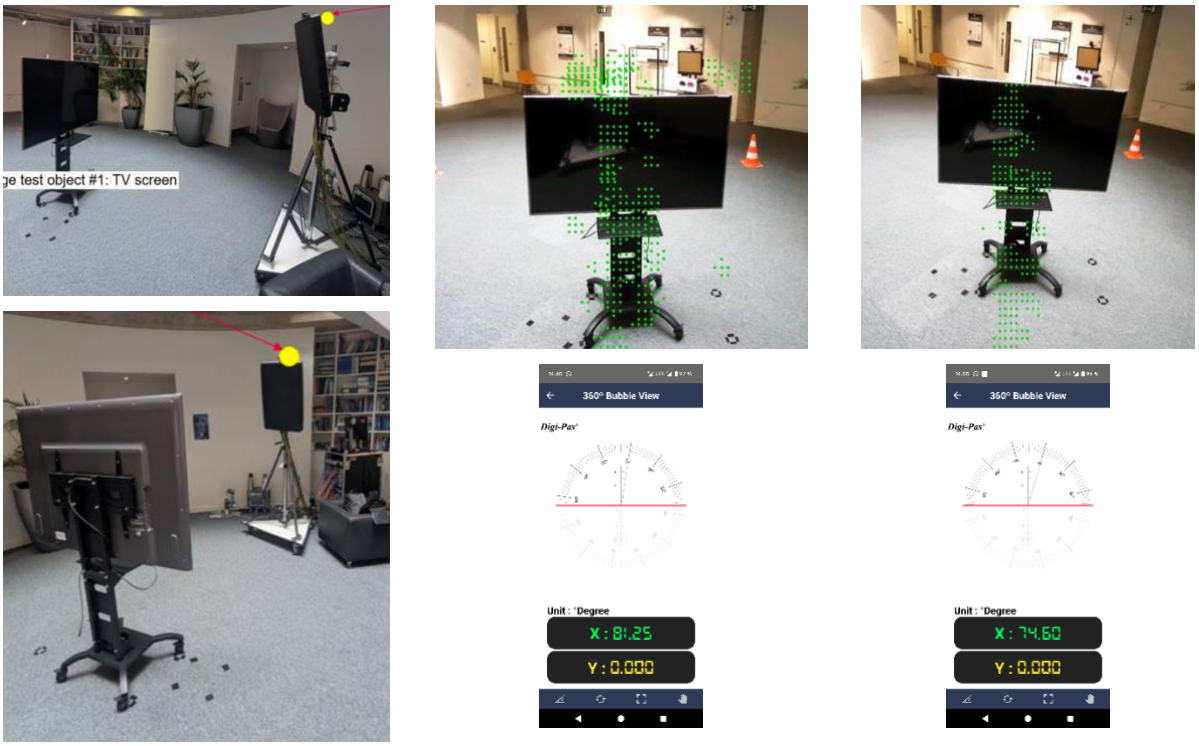
Figure 5 Representative illustration of indoor scenarios

Specifically, this indoor scenario was evaluated using two distinct target scatterers: a TV screen and a desk table, placed at a fixed distance of 3 meters from the ISAC transceiver.

Scenario #1 – TV Screen as the scatterer

By settling a typical TV screen in the laboratory environment at a fixed target distance of 3 meters, the measurements have been made to observe systematic spatial variations in point cloud reconstructions under discrete tilt angles (e.g., 81.25° and 74.60°) as seen in Figure 6-(a). Here, the detected points have been projected onto co-registered 2D RGB camera frames, as depicted in Figure 6-(b) and Figure 6-(c) for two antenna tilt positions, respectively. To analyze the 2D point cloud data extracted from Scenario #1, two alternative algorithms were implemented for ATF estimation. A high-level description of their core execution flows is presented below, with complete algorithmic details available in Annex-1.

- 2-D Cross-Correlation-Based Method (Algorithm-A): To estimate spatial shifts, a 2D Cross-Correlation approach is utilized by converting the 2D projected point cloud representations into normalized spatial intensity histograms. By evaluating the cross-correlation peak relative to the matrix center, the algorithm determines the global pixel displacement (Δx, Δy). This pixel shift is subsequently converted into an angular offset using the camera's Vertical Field of View (VFOV) and vertical image resolution, which, combined with the target distance, yields the physical vertical displacement and the corresponding antenna tilt variation.
- Column-Wise Robust Median-Based Method (Algorithm-B): Complementing the correlation approach, a Median-Based estimation method is implemented to achieve robust tilt detection against point cloud density fluctuations and uneven spatial scattering. The 2D projected point clouds are sliced along the horizontal axis into vertical strips, where the median coordinates are independently evaluated for each strip across baseline and degraded datasets. Evaluating the median shifts across corresponding strips yields a robust global pixel displacement (Δx, Δy), which is then converted into physical spatial displacement and the estimated antenna tilt angle change.



(a) Photographs from the Indoor scene (w/ TV screen case)

(b) 2D Image constructed for the ideal case (w/o ATF): Antenna angle 81.25 degrees

(c) 2D Image constructed for the erroneous case (w/ ATF): Antenna angle 74.60 degrees

Figure 6 Photographs and constructed images for indoor scenario #1: TV screen

For Scenario #1 (TV Screen) at a fixed indoor distance of 3 m, the 2D projected point clouds for the baseline (81.25°) and tilted (74.60°) antenna positions are depicted in Figure 7. The physical displacement between the two cases was successfully estimated.

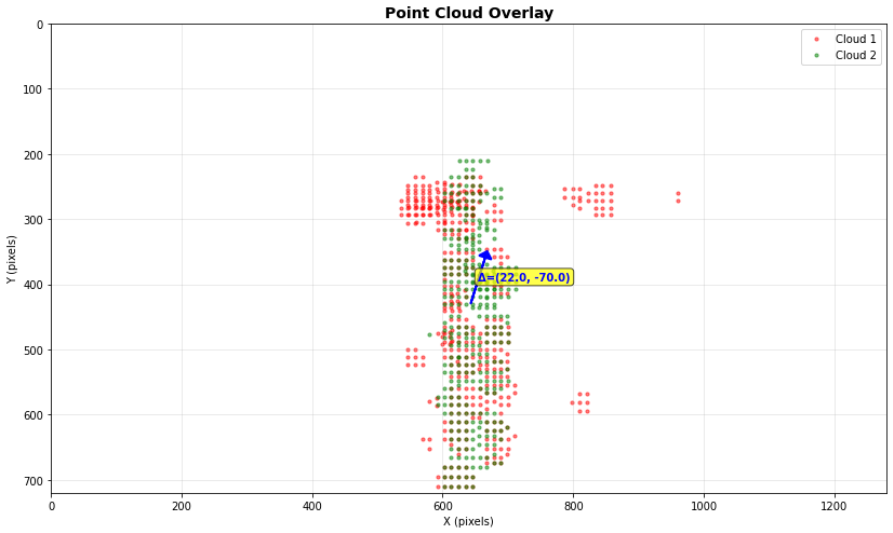
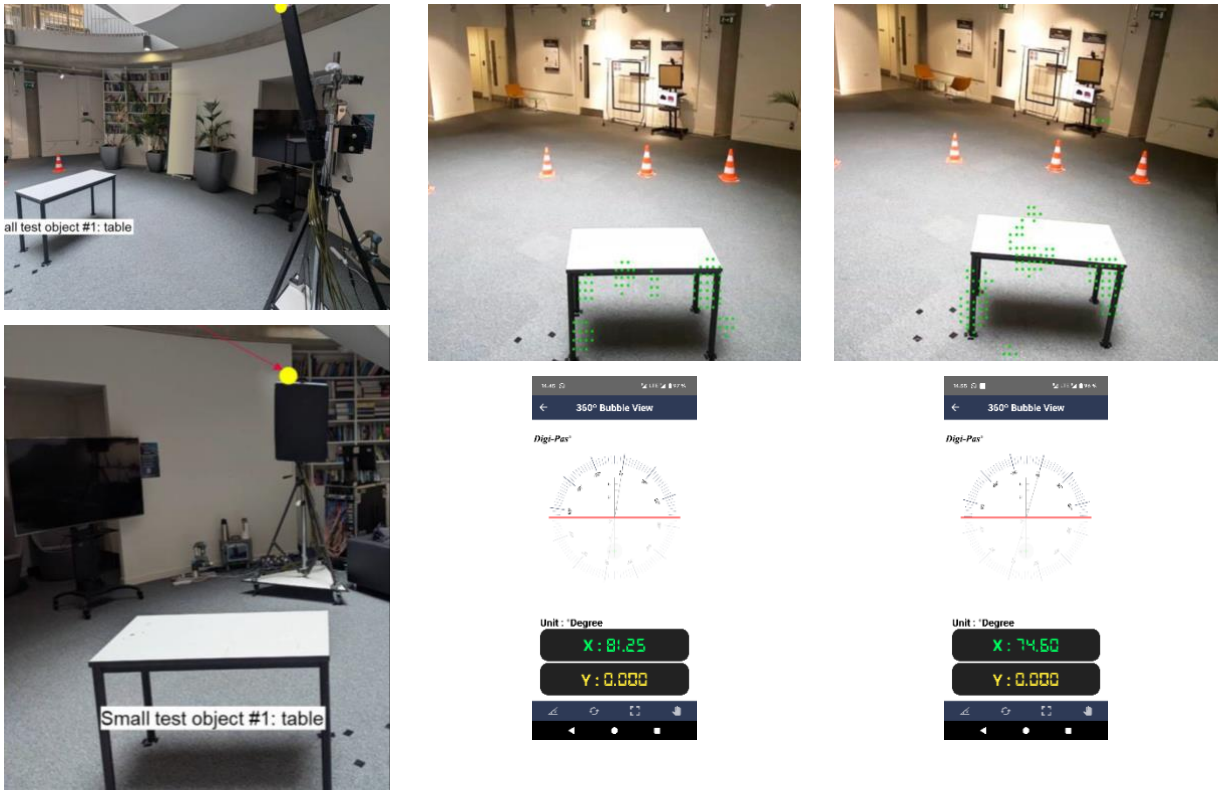


Figure 7 The overlay of projected 2D point cloud for Scenario #1

The Column-Wise Robust Median method (Algorithm-B) consistently extracted a vertical pixel shift of Δy=-70 pixels, which translates to an estimated antenna tilt angle change of -4.711° through the system's VFOV mapping. This angular discrepancy corresponds to a physical vertical displacement of -262.5 mm at a 3 m range, confirming that an upward (↑) shift in spatial point cloud coordinates indicates a downward (↓) physical ATF. Since the 2D point clouds, unlike their 3D counterparts, carry no reflection intensity, the contribution of individual points cannot be weighted, which may degrade the accuracy of antenna tilt estimation. This phenomenon is encountered in Scenario #1.

Scenario #2 – Table as the scatterer

Following a setup similar to Scenario #1, measurements were conducted using a desk table as the target scatterer positioned 3 meters from the ISAC transceiver. Point cloud variations under discrete tilt angles (81.25° vs 74.60°) were captured and projected onto 2D RGB camera frames, as illustrated in Figure 8.



(a) Photographs from the Indoor scene (w/ Table)

(b) 2D Image constructed for the ideal case (w/o ATF): Antenna angle 81.25 degrees

(c) 2D Image constructed for the erroneous case (w/ ATF): Antenna angle 74.60 degrees

Figure 8 Photographs and constructed images for indoor scenario #2: Table

For Scenario #2 (Table), the 2D projected point clouds for the baseline and tilted antenna positions are depicted in Figure 9. The Column-Wise Robust Median and 2D Cross-Correlation methods extracted a vertical pixel shift of 92.00 pixels, 100 pixels, which translates to an estimated antenna tilt angle change of -6.192°, -6.73°, respectively. This angular discrepancy corresponds to a physical vertical displacement of -345 mm and -375 mm at 3 m range, respectively, confirming that an upward (↑) shift in spatial point cloud coordinates indicates a downward (↓) physical ATF.

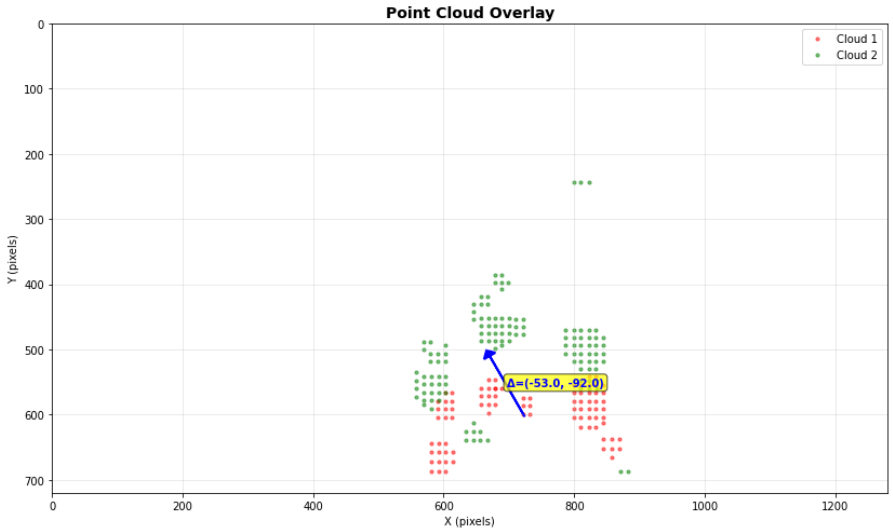


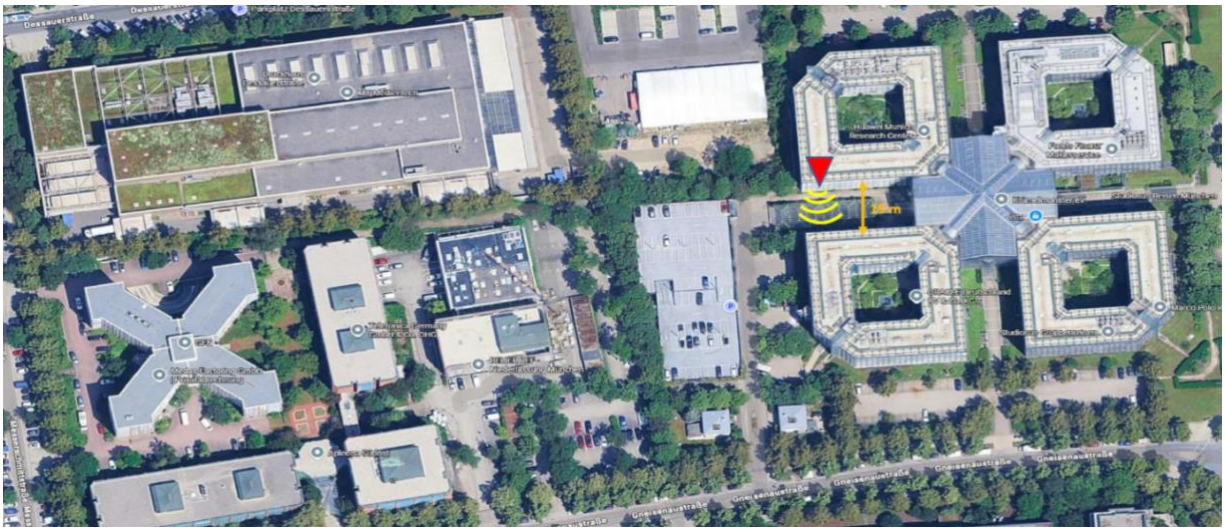
Figure 9 The overlay of projected 2D point cloud for Scenario #2

3.2. Performance-Driven Outdoor Test Campaign

Following the initial verification of the data pipeline indoors, an outdoor measurement campaign was executed at the Huawei MRC campus to evaluate diagnostic performance under representative operational propagation conditions. Since the initial indoor campaign revealed that 2D image-projected point clouds may constrain ATF estimation precision, raw 3D point cloud data were directly utilized as the primary diagnostic input for the outdoor scenarios. The outdoor setup leveraged the cmWave ISAC testbed positioned at an elevation of 15 meters to sense complex spatial surroundings across two distinct directional sectors (i.e., South and West scenarios). The performance-oriented outdoor test campaign focused on quantifying the ATF estimation has been supported by developing three distinct, sensor-free algorithmic approaches relying on 3D spatial point clouds:

- Algorithm-C: Mean-Based ATF Estimation: Serves as a low-complexity spatial baseline approach that isolates the strongest scatterers by applying an intensity margin threshold (τ_s) to eliminate background clutter. The remaining points are collapsed into a single 3D spatial mean centroid (μ_s), from which an elevation angle (θ_s) is calculated relative to the antenna height and horizontal range. The differential elevation angle between reference and tilted point clouds directly provides the estimated tilt failure ($\hat{\Delta}_\theta$).
- Algorithm-D: 3D Correlation Search: Executes a robust 3D cross-correlation search across candidate tilt angles (Ω_{search}) using a spatial fingerprint derived via DBSCAN clustering. Rotating the reference baseline point cloud around the antenna phase center pivot (a_c), the algorithm measures spatial overlap against the tilted point cloud using a Gaussian kernel weighting function (σ_{bw}). To overcome search grid discretization limits, a sub-grid parabolic refinement fits a second-order curve around the correlation peak to derive a highly refined estimate.
- Algorithm-E: Cluster Centroid Tracking and Matching: Combines density-based clustering with feature matching of intensity-weighted cluster centroids. Points surviving adaptive intensity filtering are grouped into structural clusters using DBSCAN, mapped into polar coordinates (R, ϕ, θ), and paired across baseline and tilted scenes using a combined azimuth and range cost metric. An Interquartile Range (IQR) filter isolates valid elevation discrepancies from transient environmental clutter, averaging the filtered tracks to yield the final tilt estimate ($\hat{\Delta}_\theta$).

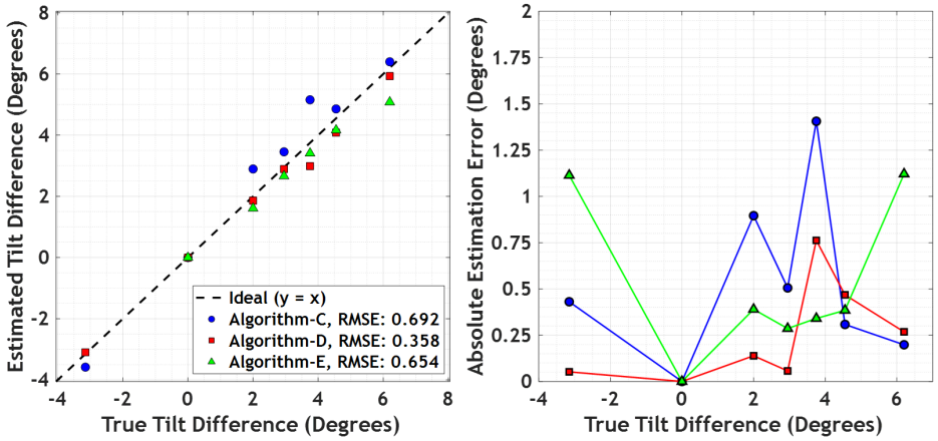
Scenario #1 – South Scene: The South Scene represents a near-field outdoor operational scenario conducted at the Huawei MRC campus to evaluate the diagnostic performance of the proposed 3D ISAC algorithms under close-range structural scattering conditions. In this setup, the cmWave testbed antenna was positioned at an elevation of 15 m, directly facing a primary building facet located at a close target range of 19 m. Physical antenna tilt failures were systematically introduced across seven discrete mechanical settings, ranging from +3.15° (uptilt) to -6.20° (downtilt), with the near-nominal setting serving as the fault-free reference baseline.



(a) Satellite view for Huawei MRC Campus – South Scene



(b) Antenna view

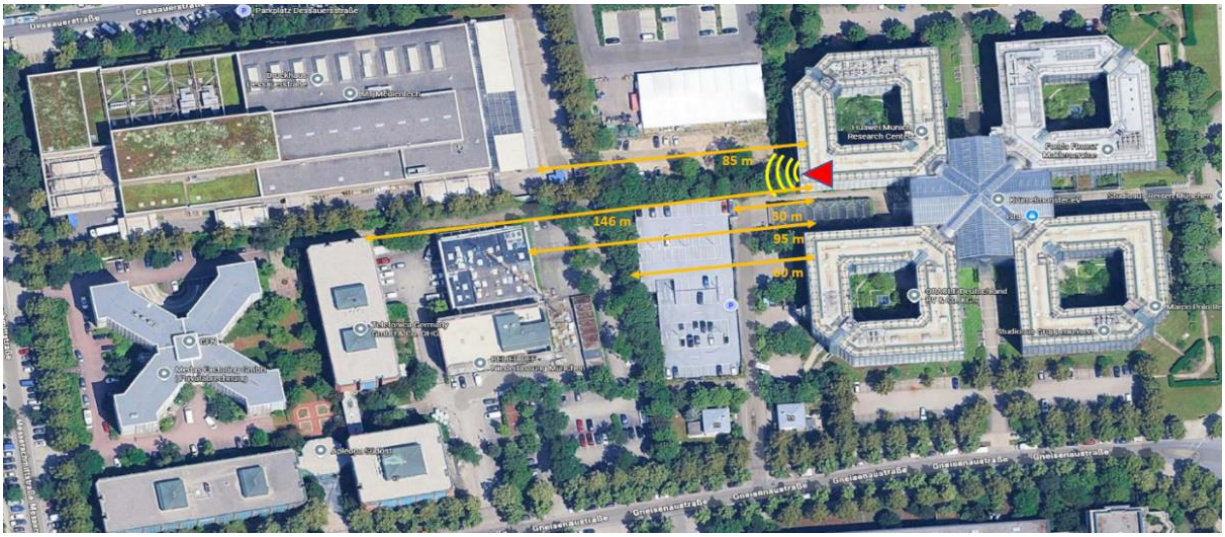


(c) Estimated values vs. ground truth (at left), absolute estimation error (at right)

Figure 10 Scenario footage and the estimation performances for the South direction

For Scenario #1 (South Scene), across seven discrete physical tilt variations, the algorithms closely tracked the ideal response trajectory, confirming that static structural features remain sufficiently invariant under local mechanical shifts. Among the evaluated approaches, the 3D Correlation Search (Algorithm-D) demonstrated better performance by achieving an RMSE of 0.358°. This accuracy is directly attributed to its holistic scene matching, Gaussian kernel weighting, and sub-grid parabolic refinement, which effectively mitigates spatial noise. In contrast, the Mean-Based (Algorithm-C) and Cluster Centroid Tracking (Algorithm-E) methods yielded RMSE values of 0.692° and 0.654°, respectively, as their reliance on collapsing clusters into single spatial centroids leaves them slightly more susceptible to stray returns. Overall, these empirical findings validate that the proposed ISAC framework can reliably detect mechanical antenna tilt anomalies with considerable precision in near-field structural environments.

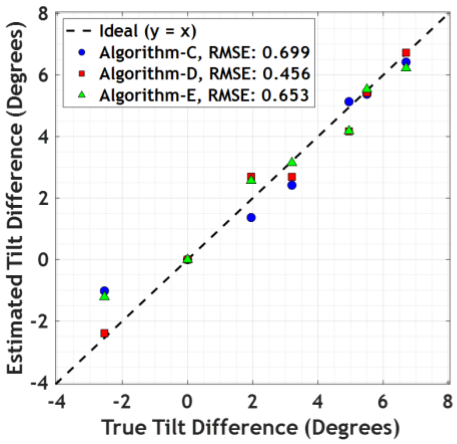
Scenario #2 – West Scene: The West Scene represents an extended-range, highly cluttered outdoor propagation scenario designed to evaluate the limits of the 3D ISAC-based ATF estimation algorithms across distant structural targets. Deployed on the same platform at the Huawei MRC campus, the testbed antenna overlooks a complex environmental topology consisting of residential buildings and dense foliage distributed between 30 m and 146 m. To analyze spatial point cloud degradation over long ranges, physical tilt failures were executed across seven discrete angular settings using the near-nominal setting as the fault-free baseline.

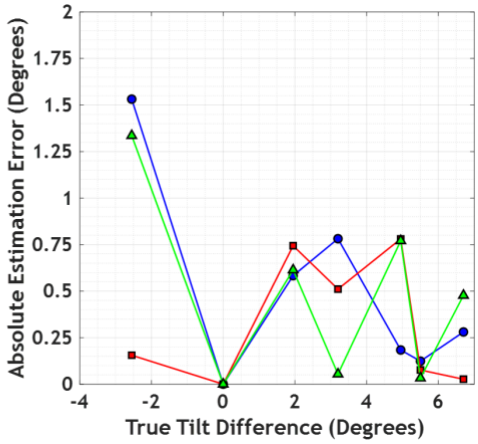


(a) Satellite view for Huawei MRC Campus – West Scene









(b) Antenna view (c) Estimated values vs. ground truth (at left), absolute estimation error (at right)

Figure 11 Scenario footage and the estimation performances for the West direction

For Scenario #2 (West Scene), the extended target range (30 m to 146 m) and the presence of dynamic environmental clutter (such as wind-induced foliage and multi-building reflections) introduced a challenging sensing setup for 3D spatial reconstruction. Despite the increased spatial dispersion of the point cloud, all three algorithms have tracked the physical tilt trend across the full angular range, proving that static structural anchors remain sufficiently reliable even at extended distances. The 3D Correlation Search (Algorithm-D) was consistently better than the baseline approach, achieving an RMSE of 0.456°. Although this represents a minor increase in estimation error compared to the near-field South Scene (0.358°), Algorithm-D demonstrated exceptional robustness by matching the entire spatial fingerprint rather than relying on isolated scatterers. On the other hand, the Mean-Based (Algorithm-A) and Cluster Centroid Tracking

(Algorithm-E) methods recorded RMSE values of $0.699°$ and $0.653°$, respectively. Because their diagnostic precision is structurally limited by the centroid reduction step, their error rates remained virtually unchanged between the near and far scenes. These findings confirm that holistic spatial correlation with sub-grid parabolic refinement is essential for achieving reliable ATF detection in complex, long-range cellular environments.

4. Business Case: Provisional Closed-Loop Roadmap and Financial Impact

Integrating the inward-facing ISAC framework for ATF estimation into commercial RAN deployments provides measurable operational efficiencies and cost reductions over conventional maintenance protocols. Existing state-of-the-art AI optimization algorithms and Remote Electrical Tilt (RET) management frameworks operate strictly within the logical and electrical domains, inherently assuming that the physical antenna infrastructure remains perfectly aligned [16] [17] [18] However, when external environmental factors – such as severe windstorms, long-term corrosion, or mechanical clamp loosening – cause unannounced physical tilt degradation, these logical optimization loops become functionally blind, attempting to optimize electrical tilt settings against physically misaligned spatial baselines [19]

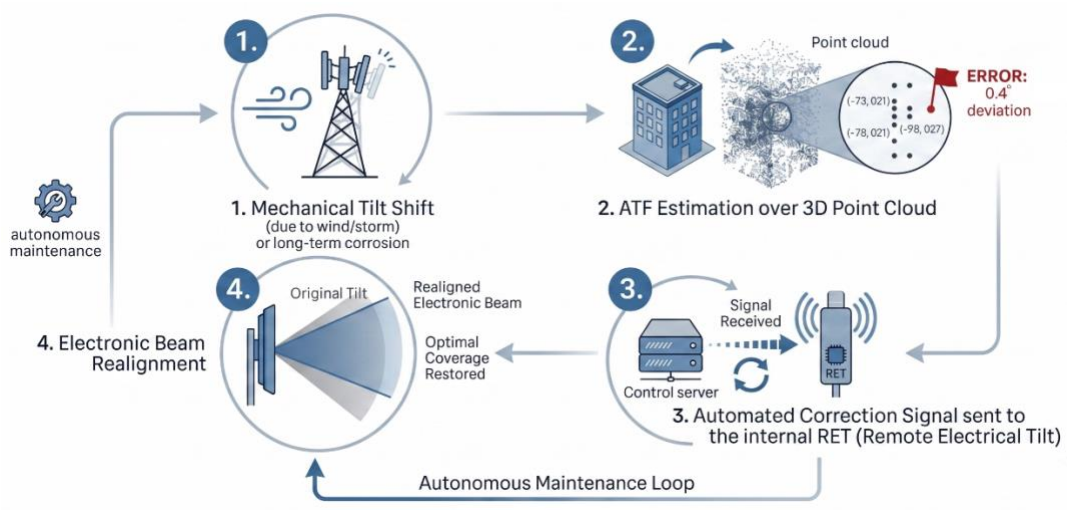


Figure 12 Closed-loop framework converting algorithmic ATF estimation into real-time RET alignment

To overcome these structural limitations, the proposed ISAC framework establishes a Provisional Closed-Loop Autonomous Maintenance Architecture, as illustrated in Figure 12, structured across four operational phases:

1. Sensing Data Acquisition: The ISAC-enabled macro base station continuously illuminates its operational sector and captures raw multi-path echoes via its existing active antenna arrays.

2. Algorithmic Processing: The co-located edge-compute engine reconstructs these echoes into a high-fidelity 3D point cloud, where advanced estimation algorithms (e.g., 3D Correlation Search) extract the physical structural drift ($\hat{\Delta}_\theta$) in real time. While stationary scatterers (geometric anchors) are almost universally present in real-world cellular sectors and dynamic clutter is effectively suppressed via standard filtering, executing 3D point cloud processing introduces a modest edge-compute resource trade-off.

3. Telemetry Integration: The calculated angular error is formatted into standardized telemetry updates and streamed directly to the network management entity (e.g., Radio Intelligent Controller) without requiring manual site audits or human intervention.

4. Automated Rectification: The estimated misalignment is converted into a compensating tilt command, applied through the RET actuator for passive antennas or through the beamforming weights for active and massive-MIMO AAUs. This targets the small deviations of a few degrees (e.g., from wind, vibration or thermal cycling) that often go unnoticed and lie within the correctable elevation range. Azimuth or roll misalignment and large mechanical failures still require a site visit. The applied offset is recorded in the sensing baseline so that the compensated state is not re-flagged.

From an economic perspective, this automated framework impacts network operational and financial advantage across two primary pillars:

- Total CAPEX Avoidance: By reusing existing transceiver hardware and spectral resources for sensing, this approach avoids the procurement, physical wiring, and maintenance associated with dedicated mechanical tracking units, 6-axis IMUs, or external IoT modules across cell sites. Furthermore, while single-point IMU sensors are susceptible to calibration drift, cannot detect panel warping, and remain insensitive to static translational displacements, the inward-facing ISAC framework provides 3D spatial awareness without requiring additional hardware components.
- Intelligent OPEX Evolution via Predictive Maintenance: Resolving physical antenna tilt degradation traditionally requires high operational expenditure (OPEX) due to periodic manual drive-tests, reactive audits following subscriber complaints, and hazardous field technician tower climbs using external optical tools like the VIAVI 3Z RF Vision Antenna Alignment Tool [20] . While effective for initial site commissioning, manual alignment tools are limited to point-in-time verification and do not provide continuous diagnostic monitoring. Substituting periodic manual audits with continuous ISAC-based monitoring supports an automated maintenance framework that identifies physical tilt deviations before coverage gaps lead to SLA violations.

In operational deployments, fault detection is formally defined by evaluating whether the estimated tilt deviation exceeds a predefined operator threshold, $\hat{\Delta}_\theta \geq \theta_{th}$ (typically set to $\theta_{th} \in [1.0°, 1.5°]$ in commercial RAN operations). Given the achieved estimation precision ($0.4°$ RMSE), this margin ensures reliable fault discrimination.

5. Limitations, Open Challenges, and Path to Production Readiness

While the experimental proof-of-concept demonstrates the fundamental feasibility of inward-facing ISAC for ATF estimation, several practical, algorithmic, and architectural challenges must be addressed before this methodology can transition into carrier-grade commercial RAN production:

1. Dimensionality Constraints in Cluttered Scenarios: Initial indoor evaluation revealed that projecting raw 3D spatial points onto 2D image planes constrains elevation estimation precision due to point compression and spatial ambiguity in dense near-field clutter. Consequently, transition to full 3D Cartesian point cloud analysis was required for the outdoor campaign. Scaling this approach to diverse macro environments necessitates robust, dimension-preserving feature extractors that maintain elevation sensitivity without excessive computational overhead.

2. Baseline Drift and Environmental Scene Dynamics: The current pipeline relies on a reference point cloud captured during an assumed fault-free state. In operational cases, stationary baselines are subject to long-term physical variations, including seasonal foliage changes, permanent structural additions (e.g., new buildings), and transient scatterers (e.g., parked heavy vehicles). Establishing robust baseline update policies - such as rolling temporal averaging and statistical median filtering - is essential to prevent slow environmental evolution from triggering false tilt alarms.

3. ISAC Operation over Commercial TDD AAUs: Commercial 5G/6G Massive MIMO Active Antenna Units (AAUs) are heavily optimized for TDD communications traffic. Embedding sensing slots within commercial frame structures introduces fundamental trade-offs between sensing duty cycle, transmit power allocation, and user throughput. Furthermore, isolating self-interference and inward-facing antenna coupling within existing TDD radio frequency (RF) front-ends requires dedicated hardware calibration or digital cancellation schemes.

4. Edge Computational Complexity and Memory Overhead: Generating high-fidelity 3D point clouds and executing continuous spatial correlation searches impose non-negligible compute loads. To operate without degrading real-time scheduler performance, these algorithms must be integrated efficiently into co-located BBUs or edge-based Near-Real-Time RAN Intelligent Controllers (Near-RT RICs) through hardware-accelerated, lightweight processing pipelines.

5. Coupled Multi-Axis Misalignment (Azimuth and Roll): The experimental campaign focused on isolated vertical tilt failure. However, extreme weather conditions frequently induce coupled three-dimensional mechanical deformations, including azimuthal twisting and structural roll. Extending the correlation search to a simultaneous 3-DoF (degrees of freedom) pose-estimation framework requires larger search spaces and enhanced angular resolution along all coordinate axes.

6. Standardization and Management Interfaces: Enabling automated closed-loop mitigation across multi-vendor networks necessitates standardizing the telemetry and control feedback. Specifically, defining standardized open interfaces (e.g., extensions to the O-RAN E2 and O1 service models) is imperative to stream quantified mechanical misalignment metrics from the ISAC processing unit to the RIC and subsequently issue autonomous RET correction commands.

6. Conclusions

This Technical Report has presented a joint one6G Working Group 4 Proof of Concept (PoC) demonstrating autonomous, sensor-free physical antenna tilt failure diagnosis enabled by Integrated Sensing and Communication (ISAC). By processing 3D Point Cloud spatial returns captured via the cmWave ISAC testbed engineered by Huawei Munich Research Centre, Turkcell 6GEN.LAB successfully evaluated diagnostic algorithms capable of isolating mechanical tilt anomalies with considerable angular precision.

The inward-facing ISAC paradigm validated in this work establishes a solid foundation for zero-touch, self-healing Radio Access Networks (RAN). By automating infrastructure health monitoring, cellular operators can significantly reduce Operational Expenditure (OPEX), eliminate high-risk manual tower inspections, and maintain optimal Quality of Service (QoS). The open publication of the underlying dataset under the ODC-By license actively supports standardized 6G research and development within the one6G ecosystem.

Building upon the baseline performances established in this study, future work will focus on developing advanced Artificial Intelligence (AI) and Machine Learning (ML)-based estimation frameworks designed to push diagnostic accuracy further, targeting estimation errors below $0.1°$. Additionally, efforts will be directed toward integrating these autonomous diagnostic and estimation capabilities directly into the real-time edge-computing unit of the cmWave ISAC testbed. This integration will enable fully automated, on-device telemetry extraction, paving the way for instantaneous closed-loop RET realignment in commercial 6G deployments.

Acknowledgments

This technical report and the underlying PoC activities were conducted within the framework of Working Group 4 [1] (WI404) under the one6G association. The authors would like to acknowledge the collaborative effort between Turkcell 6GEN.LAB and Huawei Munich Research Centre (MRC).

Special thanks are extended to all contributors and member organizations of one6G for supporting the open data initiative. The experimental 3D Point Cloud dataset utilized in this work is hosted on the one6G repository under the Open Data Commons Attribution License (ODC-By).

Contributors

Ahmet Faruk Coşkun (Turkcell), coskun.ahmet@turkcell.com.tr

Batuhan Kaplan (Turkcell), batuhan.kaplan@turkcell.com.tr

Emre Arslan (Turkcell), emre.arslan@turkcell.com.tr

Hanwen Cao (Huawei), Hanwen.Cao@huawei.com

Josef Eichinger (Huawei), Joseph.Eichinger@huawei.com

Mohamed Gharba (Huawei), mohamed.gharba@huawei.com

Samed Keşir (Turkcell), samed.kesir@turkcell.com.tr

7. Annex: Flowcharts and Detailed Steps of ATF Estimation Algorithms

In this section, the step-by-step algorithmic workflows developed for the Antenna Tilt Failure (ATF) detection and estimation process are detailed. These algorithms leverage the $N \times 4$ spatial point cloud matrices generated by the cmWave ISAC testbed – comprising 3D coordinates (x, y, z) and radar scattering intensities (σ) – to evaluate physical antenna tilt degradation. The following subsections outline the underlying mathematical logic and sequential processing steps for each proposed approach.

7.1. Annex-1: Algorithms Developed for Indoor Dataset

This annex provides the detailed mathematical logic, processing steps, and algorithmic workflows for the 2D point cloud post-processing methods evaluated during the indoor test campaign. Developed for baseline verification and initial proof-of-concept validation, these algorithms process 2D spatial point cloud representations projected onto co-registered camera frames to quantify physical ATF. By analyzing spatial point distributions generated across controlled scatterers (e.g., TV screen and table targets at a 3 m range), the proposed approaches translate pixel-level spatial shifts into precise physical vertical displacements and corresponding angular tilt deviations.

7.1.1. Algorithm-A: 2D Cross-Correlation-Based ATF Estimation

Algorithm-A determines physical antenna tilt failure by evaluating the two-dimensional spatial cross-correlation peak between normalized intensity histograms derived from projected 2D point clouds. The explicit processing steps, mathematical formulations, and operational logic are detailed in Table 1.

Table 1 Algorithm-A: 2D Cross-Correlation-Based ATF Estimation

Line	Phase / Description	Mathematical Formulation / Operation
Input	Pre-loaded 2D projected point clouds	$\mathbf{P}_{ref}, \mathbf{P}_{tilt} \in \mathbb{R}^{N\times 2}$ (Frame size: 1280×720 px)
Input	Target distance & Vertical Field of View	$d = 3.0$ m, VFOV
Output	Estimated physical tilt angle change & physical shift	$\widehat{\Delta}_{\theta}$ (degrees), $\Delta \mathrm{Y}_{mm}$ (mm)
1	Histogram Generation	Convert point clouds into 128×72 spatial intensity histograms: $\mathbf{H}_{ref}, \mathbf{H}_{tilt} \leftarrow \mathrm{Hist2D}(\mathbf{P}, \mathrm{bins} = [128,72])$
2	Intensity Normalization	Normalize maps to unit peak intensity: $\mathbf{H}_{norm} = \mathbf{H}/\max(\mathbf{H})$
3	2D Cross-Correlation	Compute spatial cross-correlation map: $\mathbf{R}(\Delta x, \Delta y) = \mathbf{H}_{ref,norm} \otimes \mathbf{H}_{tilt,norm}$

Line	Phase / Description	Mathematical Formulation / Operation
4	Peak Detection	Extract global shift relative to correlation center: $(\Delta x, \Delta y) = \arg\max(\mathbf{R}) - \text{Center}$
5	Pixel-to-Angle Conversion	Map vertical pixel displacement through VFOV: $\widehat{\Delta}_\theta = \frac{180}{\pi}\arctan\left(\frac{\Delta y \cdot \text{VFOV}}{\text{Height}_{\text{px}}}\right)$
6	Physical Shift Calculation	Compute physical vertical displacement at distance d: $\Delta Y_{mm} = d \cdot \tan(\widehat{\Delta}_\theta) \times 1000$
7	Directional Mapping	Map shift direction (↑ point cloud shift ⇒ ↓ physical antenna tilt)
8	Return Output	return $\widehat{\Delta}_\theta, \Delta Y_{mm}, (\Delta x, \Delta y)$

7.1.2. Algorithm-B: Column-Wise Robust Median-Based ATF Estimation

Algorithm-B isolates antenna tilt failure by slicing projected point clouds into vertical strips and computing column-wise median spatial shifts. This robust statistical treatment ensures insulation against point cloud density variations and localized scatterer noise. The mathematical sequence is outlined in Table 2.

Table 2 Algorithm-B: Column-Wise Robust Median-Based ATF Estimation

Line	Phase / Description	Mathematical Formulation / Operation
Input	Pre-loaded baseline and tilted point clouds	$\mathbf{P}_{ref}, \mathbf{P}_{tilt} \in \mathbb{R}^{N\times 2}$ (Frame size: 1280×720 px)
Input	Target distance & Vertical Field of View	$d = 3.0$ m, VFOV
Output	Robust tilt angle change & physical displacement	$\widehat{\Delta}_\theta$ (degrees), ΔY_{mm} (mm)
1	Horizontal Slicing	Slice point clouds along X-axis into M vertical strips
2	Loop Initialization	**foreach** vertical strip $m \in \{1,2,\dots,M\}$ **do**
3	Strip Median Evaluation	Evaluate Y-axis medians: $\mu_{y,ref}^{(m)} = \text{median}(\mathbf{P}_{ref}^{(m)}(y)), \mu_{y,tilt}^{(m)} = \text{median}(\mathbf{P}_{tilt}^{(m)}(y))$
4	Strip Shift Computation	Compute local vertical discrepancy: $\delta_y^{(m)} = \mu_{y,tilt}^{(m)} - \mu_{y,ref}^{(m)}$
5	End Loop	**end**
6	Global Shift Extraction	Extract global robust pixel shift: $\Delta \text{y} = \text{median}\left(\left\{\delta_y^{(1)}, \delta_y^{(2)}, \dots, \delta_y^{(M)}\right\}\right)$
7	Horizontal Shift Calculation	Compute overall X-axis offset: $\Delta x = \text{median}(\mathbf{P}_{tilt}(x)) - \text{median}(\mathbf{P}_{ref}(x))$
8	Angular & Physical Conversion	Compute physical vertical displacement at distance d: $\Delta Y_{mm} = d \cdot \tan(\widehat{\Delta}_\theta) \times 1000$
9	Return Output	return $\widehat{\Delta}_\theta, \Delta Y_{mm}, (\Delta x, \Delta y)$

7.2. Annex-2: Algorithms Developed for Outdoor Dataset

This annex provides the detailed mathematical formulations, pseudocode workflows, and structural execution steps for the three point cloud-based ATF estimation algorithms evaluated in the outdoor test campaigns (South and West scenarios). All algorithms process $N \times 4$ multi-dimensional tuples $p_k=[x_k, y_k, z_k, \rho_k]$ representing 3D spatial coordinates and scattering reflectivity generated by the monostatic cmWave ISAC testbed.

7.2.1. Algorithm-C: Mean-Based ATF Estimation

Algorithm-C provides a low-complexity spatial baseline by deriving trigonometric elevation angles from the arithmetic centroids of high-scattering point cloud returns. The underlying mathematical formulations, logical sequence, and execution phases for Algorithm-C are explicitly detailed in Table 3.

Table 3 Algorithm-C: Mean-Based ATF Estimation

Line	Phase / Description	Mathematical Formulation / Operation
Input	Pre-loaded point cloud structures	$\mathbf{D}_{ref}$, $\mathbf{D}_{tilt}$ (3D coordinates $\boldsymbol{l}$ and intensities $\boldsymbol{\rho}$)
Input	Base station antenna height	$h_{BS} = 15$ m
Input	Threshold scaling margin multiplier	γ_{margin}
Output	Estimated physical antenna tilt failure magnitude	$\widehat{\Delta}_\theta$ (degrees)
1	Loop Initialization	**foreach** scenario $s \in \{\text{reference}, \text{tilted}\}$ **do**
2	Data Extraction	Extract coordinates and intensities: $\mathbf{D}_s \rightarrow (\boldsymbol{l_s}, \boldsymbol{\rho}_s)$
3	Coordinate Inversion	Invert vertical coordinates to correct ground mapping: $\mathbf{Z}_s \leftarrow -\mathbf{Z}_s$
4	*Intensity-Based Spatial Filtering*	Compute dynamic threshold: $\tau_s \leftarrow \gamma_{margin} \times \max\{\boldsymbol{\rho}_s\}$
5	Filtering Low-Scattering Points	Filter point cloud: $\mathbf{P}_s \leftarrow \{\mathbf{x} \in \boldsymbol{l_s} \mid \boldsymbol{\rho}_s(\mathbf{x}) > \tau_s\}$
6	*Arithmetic Spatial Mean*	Compute 3D spatial mean centroid: $\mu_s \leftarrow \text{mean}(\mathbf{P}_s)$
7	*Elevation Angle Derivation*	Height difference relative to BS: $\Delta z_s \leftarrow \mu_s(z) - h_{BS}$
8	Horizontal Distance Derivation	Calculate distance: $d_{h,s} \leftarrow \sqrt{\mu_s^2(x) + \mu_s^2(y)}$
9	Elevation Angle Calculation	Compute angle: $\theta_s \leftarrow \frac{180}{\pi} \arctan\left(\frac{\Delta z_s}{d_{h,s}}\right)$
10	End Loop	**end**
11	*Final ATF Extraction*	Calculate net angular shift: $\widehat{\Delta}_\theta \leftarrow \theta_{ref} - \theta_{tilted}$
12	Return Output	**return** $\widehat{\Delta}_\theta$

Following the parameter pipeline outlined in the table above, the optimal configuration for Algorithm-C is achieved in the South scenario with an intensity threshold of $\gamma_{th} = 0.9$, histogram-based thresholding enabled, and unweighted coordinates, whereas the West scenario requires $\gamma_{th} = 0.6$ with histogram thresholding disabled and intensity-weighted coordinates.

7.2.2. Algorithm-D: 3D Correlation Search

Algorithm-D executes a brute-force spatial rotation search across candidate angles followed by sub-grid parabolic fitting to achieve considerable tilt estimation accuracy.

Table 4 Algorithm-D: 3D Correlation Search

Line	Phase / Description	Mathematical Formulation / Operation
Input	Baseline and compromised point clouds	$\mathbf{D}_{ref}, \mathbf{D}_{tilt}$ (3D coordinates $\boldsymbol{l}$ and intensities $\boldsymbol{\rho}$)
Input	Intensity and DBSCAN parameters	$\gamma, \epsilon, m_{pts}$
Input	Angular search bounds and step size	$\Omega_{search}, \delta_\theta$
Input	Spatial correlation bandwidth	σ_{bw}
Output	Refined antenna tilt failure estimation	$\widehat{\Delta}_\theta$
1	Spatial Fingerprinting	Filter reference baseline: $\mathbf{P}_{ref} \leftarrow \mathrm{FilterClusters}(\mathrm{DBSCAN}(\mathbf{D}_{ref}, \epsilon, m_{pts}), \gamma)$
2	Rotation Pivot Calculation	Compute antenna phase center of mass: $a_c \leftarrow \mathrm{CenterOfMass}(l_{tx})$
3	Filter Compromised Data	Filter tilted point cloud: $\mathbf{P}_{tilt} \leftarrow \mathrm{FilterClusters}(\mathrm{DBSCAN}(\mathbf{D}_{tilt}, \epsilon, m_{pts}), \gamma)$
4	3D Search Loop	for each candidate angle $\theta_j \in \Omega_{search}$ with step δ_θ do
5	Apply 3D Rotation	Apply tilt rotation: $\mathbf{P}_{rot} \leftarrow \mathrm{ApplyTiltRotation}(\mathbf{P}_{ref}, a_c, \theta_j)$
6	Calculate 3D Correlation	Compute metric: $\mathbf{S}(j) \leftarrow \mathrm{Calculate3DCorrelation}(\mathbf{P}_{rot}, \mathbf{P}_{tilt}, \sigma_{bw})$
7	End Loop	end
8	Coarse Peak Extraction	Find peak correlation index: $k \leftarrow \mathrm{argmax}(\mathbf{S}) \Longrightarrow \widehat{\Delta}_\theta \leftarrow \theta_k$
9	*Sub-Grid Parabolic Refinement*	if $1 < k < \mathrm{length}(\mathbf{S})$ then
10	Parabola Fitting	Fit 2nd-order parabola: $y = p_1 x^2 + p_2 x + p_3$ over $\mathbf{S}(\mathrm{k}-1{:}\,\mathrm{k}+1)$
11	Concavity Check	if $p_1 < 0$ then
12	Vertex Calculation	Compute peak: $\theta_{refined} \leftarrow -p_2/(2p_1)$
13	Boundary Validation	if $\lvert\theta_{refined} - \widehat{\Delta}_\theta\rvert < 2\delta_\theta$ then

Line	Phase / Description	Mathematical Formulation / Operation
14	Update Estimate	$\widehat{\Delta}_\theta \leftarrow \theta_{refined}$
15-17	End Ifs	end / end / end
18	Return Output	return $\widehat{\Delta}_\theta$

Following the parameter pipeline outlined in the table above, the optimal configuration for Algorithm-D in the South scenario employs an intensity threshold of $\gamma_{th} = 0.55$, clustering bounds of $\epsilon = 3.5$ m, $m_{pts} = 16$, angular correlation bandwidth of $\sigma_{bw} = 2.5$, whereas the West scenario optimizes at $\gamma_{th} = 0.45$, clustering bounds of $\epsilon = 3.0$ m, $m_{pts} = 10$, angular correlation bandwidth of $\sigma_{bw} = 3.5$.

7.2.3. Algorithm-E: Cluster Centroid Tracking and Matching

Algorithm-E utilizes feature matching of density-weighted cluster centroids combined with Interquartile Range (IQR) statistical insulation to eliminate dynamic outliers.

Table 5 Algorithm-E: Cluster Centroid Tracking and Matching for ATF Estimation

Line	Phase / Description	Mathematical Formulation / Operation
Input	Baseline and tilt-compromised structures	$\mathbf{D}_{ref}, \mathbf{D}_{tilt}$ (3D coordinates $\boldsymbol{l}$ and intensities $\boldsymbol{\rho}$)
Input	Intensity threshold factors	γ_1, γ_2
Input	DBSCAN core density parameters	ϵ, m_{pts}
Input	Matching constraints	$\mathbf{C}_{bounds} = [\Delta\phi_{max}, \Delta R_{max}, \mathrm{Cost}_{max}]$
Output	Outlier-insulated tilt failure estimation	$\widehat{\Delta}_\theta$
1	Point Cloud Filtering	Filter raw points: $\mathbf{P}_{ref} \leftarrow \mathrm{FilterPoints}(\mathbf{D}_{ref}, \gamma_1)$ and $\mathbf{P}_{tilt} \leftarrow \mathrm{FilterPoints}(\mathbf{D}_{tilt}, \gamma_2)$
2	Density Clustering	Cluster points: $\mathbf{U}_{ref} \leftarrow \mathrm{DBSCAN}(\mathbf{P}_{ref}, \epsilon, m_{pts})$ and $\mathbf{U}_{tilt} \leftarrow \mathrm{DBSCAN}(\mathbf{P}_{tilt}, \epsilon, m_{pts})$
3	Weighted Centroid Extraction	Compute intensity-weighted centroids μ_{ref} for qualified baseline clusters
4	Polar Coordinates Mapping	Map centroids to polar profiled: $\Omega_{ref} \leftarrow [\mathbf{R}_{ref}, \mathbf{\Phi}_{ref}, \mathbf{\Theta}_{ref}]$
5	Compromised Centroids	Compute intensity-weighted centroids μ_{tilt} for all discovered compromised clusters
6	Nearest-Neighbor Matching	foreach reference centroid $i \in \mu_{ref}$ do
7	Spatial Cost Evaluation	Calculate spatial cost metric: $\mathrm{Cost}(j) = \beta_\phi \lvert\phi_i - \phi_j\rvert + \beta_R \left(\frac{R_i - R_j}{R_i}\right), \forall j \in \mu_{tilt}$
8	Minimum Cost Selection	Find best candidate match: $k \leftarrow \mathrm{argmin}(\mathrm{Cost})$

Line	Phase / Description	Mathematical Formulation / Operation
9	Constraint Validation	if $\mathbf{Cost}(k) < \mathbf{Cost}_{max}$ and angular/range shifts satisfy $\mathbf{C}_{bounds}$ then
10	Local Discrepancy Calculation	Calculate elevation shift: $\delta_\theta \leftarrow \theta_i - \theta_k$
11	Accumulate Valid Tracks	Append to discrepancy list: $\mathbf{\Delta}_\theta \leftarrow [\mathbf{\Delta}_\theta;\ \delta_\theta]$
12	End Loop	end / end
13	IQR Outlier Insulation	Compute distribution percentiles: $Q_1 \leftarrow \mathbf{prctile}(\mathbf{\Delta}_\theta, 25)$ and $Q_3 \leftarrow \mathbf{prctile}(\mathbf{\Delta}_\theta, 75)$
14	Calculate IQR Range	Compute Interquartile Range: $\mathbf{IQR} \leftarrow Q_3 - Q_1$

Following the parameter pipeline outlined in the table above, the optimal configuration for Algorithm-E in the South scenario uses an intensity threshold of $\gamma_{th} = 0.50$, clustering constraints of $\epsilon = 3.0$ m, $m_{pts} = 10$, spatial association limits of $\Delta\phi_{max} = 6°$, $\Delta R_{max} = 0.1$ m, and $\Delta C_{max} = 8.0$, whereas the West scenario optimizes at $\gamma_{th} = 0.60$, $\epsilon = 3.5$, $m_{pts} = 10$, spatial association limits of $\Delta\phi_{max} = 6°$, $\Delta R_{max} = 0.2$ m, and $\Delta C_{max} = 8.0$.

Acronyms

3GPP	3rd Generation Partnership Project
6G	Sixth Generation of Mobile Communication System
AAU	Active Antenna Unit
AI	Artificial Intelligence
ATF	Antenna Tilt Failure
BBU	Baseband Unit
BS	Base Station
CAPEX	Capital Expenditure
CSI	Channel State Information
DBSCAN	Density-Based Spatial Clust. of Applications with Noise
ETSI	European Telecommunications Standards Institute
FoV / VFoV	Field of View / Vertical Field of View
I/Q	In-phase and Quadrature
IQR	Interquartile Range
ISAC	Integrated Sensing and Communication
MIMO	Multiple-Input Multiple-Output
MRC	Munich Research Centre
ODC-By	Open Data Commons Attribution License
OFDM	Orthogonal Frequency Division Multiplexing
OPEX	Operational Expenditure
PC	Point Cloud
PoC	Proof of Concept
QoS	Quality of Service
RAN	Radio Access Network
RET	Remote Electrical Tilt
RF	Radio-Frequency
RIC	RAN Intelligent Controllers
RMSE	Root Mean Square Error
SCS	Subcarrier Spacing
SLA	Service Level Agreement
TDD	Time-Division Duplex
TRX	Transceiver / Transmit-Receive Element
UE	User Equipment

References

[1] one6G Association, One6G.org, one6g.org/working-groups/working-group-4

[2] S. Schwarz and S. Pratschner, “Multiple antenna systems in mobile 6G: Directional channels and robust signal processing,” IEEE Communications Magazine, vol. 61, no. 4, pp. 64–70, 2023.

[3] D. Witkowski and J. Vetter, “RF antenna misalignment effects on 4G/LTE data throughput,” Sunsight Technical White Paper, 2016.

[4] P. Donegan, “Mobile network outages & service degradations: A heavy reading survey analysis,” Firmenschrift, Heavy Reading, 2013.

[5] A. Sibila, “Smart macro network enhancements: Antenna tilt optimization (part 3),” Rohde & Schwarz Stories & Insights, 2024.

[6] D. Mulvey, C. H. Foh, M. A. Imran, and R. Tafazolli, “Cellular network antenna tilt anomaly detection using federated unsupervised learning,” in IEEE ICC 2023, IEEE, 2023, pp. 3048–3053.

[7] N. Seifi, M. Coldrey, M. Matthaiou, and M. Viberg, “Impact of base station antenna tilt on the performance of network MIMO systems,” in 2012 IEEE 75th VTC Spring, IEEE, 2012, pp. 1–5.

[8] S. K. Yong, M. E. Sahin, and Y. H. Kim, “On the effects of misalignment and angular spread on the beamforming performance,” Proc. IEEE CCCN, pp. 1–5, 2007.

[9] S. Kesir, B. Kaplan, E. Arslan and A. F. Coskun, "Antenna Tilt Failure Detection and Estimation via Integrated Sensing and Communications," 2026 EuCNC, Malaga, Spain, 2026, pp. 797-802.

[10] J. Yang, C.-K. Wen, X. Li, and S. Jin, “RIS-aided cooperative ISAC networks for structural health monitoring,” IEEE Journal on Selected Areas in Communications, 2025.

[11] WG4 of One6G Association, “Test case description of the PoC about Detection of Antenna Tilt Failures”, one6G.org internal specification https://shared.one6g.org/index.php/f/124200

[12] M. Gharba, “6G ISAC-Based Environmental Sensing”, one6G Open Lecture #12, April 23rd 2026, https://one6g.org/one6g-open-lecture-12-experimental-technologies-for-6g-toward-network-intelligence-event-report/

[13] Z. et al., “6G ISAC enables environment object reconstruction,” IEEE Journal of Selected Topics in Electromagnetics, Antennas and Propagation, vol. 1, no. 1, pp. 165–178, 2025.

[14] Y. Ding and D. C. J. Munson, “A fast back-projection algorithm for bistatic SAR imaging,” Proc. Int. Conf. Image Process., 2002.

[15] Digi-Pas Technologies, "DWL-90Pro: 2-Axis Pocket-Size Digital Level," Technical Product Datasheet, Digi-Pas USA / JSB Tech, 2026.

[16] B. Partov, D. J. Leith, and R. Razavi, “Utility fair optimization of antenna tilt angles in LTE networks,” IEEE/ACM Transactions on Networking, vol. 23, no. 1, pp. 175–185, Feb. 2015.

[17] E. Aumayr, S. Feghhi, F. Vannella, E. A. Hakim, and G. Iakovidis, “A safe reinforcement learning architecture for antenna tilt optimisation,” arXiv preprint arXiv:2012.01296, 2020.

[18] N. Dandanov, H. Al-Shatri, A. Klein, and V. K. Poulkov, “Dynamic self-optimization of the antenna tilt for best trade-off between coverage and capacity in mobile networks,” Wireless Personal Communications, vol. 92, no. 1, pp. 251–278, 2017.

[19] L. Jia et al., “Analysis of the influence of antenna arrangement parameters on the aerodynamic performance of telecommunication towers,” Applied Sciences, vol. 14, no. 6, p. 2538, 2024.

[20] VIAVI Solutions, "RF Vision Antenna Alignment Tool," Technical Product Specification, VIAVI Solutions Inc., San Jose, CA, USA, 2026. [Online]. Available: https://www.viavisolutions.com/en-us/products/rf-vision